17th International Symposium on Ice
Saint Petersburg, Russia, 21 - 25 June 2004
International Association of Hydraulic Engineering and Research

NUMERICAL SIMULATION OF SEA ICE GROWTH AND DESALINATION

Chris Petrich[1], Pat J. Langhorne[1], Zhifa Sun[1]

ABSTRACT
We present a numerical model based on the finite volume method to simulate sea ice growth and desalination as a flow process through a porous medium with phase change. To achieve this we estimate a permeability-porosity relationship for the initial stages of sea ice growth from experimental data for brine drainage. The model generates ice sheets with salinity profiles close to calculations based on ice growth velocity.

INTRODUCTION
It is often desirable to know the permeability of sea ice to understand microscopic processes inside ice sheets that affect the salt budget during sea ice formation [17, 7], or the meltwater budget during sea ice disintegration [6]. Direct measurements of the permeability as a function of surface temperature [14], porosity [6, 8] or microstructure [8] are difficult to obtain and are thus scarce. They show a considerable amount of scatter that is attributed, in part, to sample size effects [8]. They reveal the sensitivity of flow resistance to the crystal structure and history of a sea ice sheet. For large scale modelling purposes it can be desirable to find a simple parameterisation of the permeability of sea ice that accounts implicitly for small scale fluctuations [6]. We present an attempt to find a permeability function that is suitable for modelling sea ice growth. Numerical simulations are performed that illustrate the capability of a simple permeability-porosity function to generate realistic sea ice sheet salinity profiles during ice growth.

MODEL DESCRIPTION
We treat sea ice growth as the flow of a Newtonian fluid in a two-dimensional domain that is partly pure liquid, and partly porous ice. The solid matrix of the porous medium is stationary in position, but time variable as governed by the phase change. The governing equations reduce to the Navier-Stokes equations with Boussinesq approximation in the liquid region, while flow in the porous medium is dominated by friction that is expressed through a term after Darcy [5]. Permeability is treated as a

[1] University of Otago, Physics Department, Dunedin, New Zealand
e-mail: pjl@physics.otago.ac.nz

function of local porosity. The porous medium undergoes phase change, and local thermodynamic equilibrium is assumed. The numerical implementation is based on the finite volume method with a staggered rectangular grid [12].

The governing equations of the finite volume method are volume-averaged formulations of the Navier-Stokes equations for a pure liquid. We chose the integration volume to be large enough so that small changes in position cause only small changes in average properties. We use a governing set of equations that is valid if all physical properties of the pure liquid and of the pure solid are constant in time and independent of position. In the momentum equations we apply the Boussinesq approximation, i.e. the density of the liquid is constant except in the buoyancy term, where it is treated as a function of local temperature and salinity.

The volume averaged momentum and mass conservation equations for a no-slip boundary condition between microscopic solid and liquid are

$$\rho_l\left[\frac{\partial fu}{\partial t}+fu\frac{\partial u}{\partial x}+fv\frac{\partial u}{\partial y}\right]=\mu\left[\frac{\partial^2 fu}{\partial x^2}+\frac{\partial^2 fu}{\partial y^2}\right]-f\frac{\partial p}{\partial x}+f\rho g_x-f\frac{\mu}{\Pi_x}fu\,, \tag{1}$$

$$\rho_l\left[\frac{\partial fv}{\partial t}+fu\frac{\partial v}{\partial x}+fv\frac{\partial v}{\partial y}\right]=\mu\left[\frac{\partial^2 fv}{\partial x^2}+\frac{\partial^2 fv}{\partial y^2}\right]-f\frac{\partial p}{\partial y}+f\rho g_y-f\frac{\mu}{\Pi_y}fv\,, \tag{2}$$

$$\left(1-\frac{\rho_s}{\rho_l}\right)\frac{\partial f}{\partial t}+\frac{\partial fu}{\partial x}+\frac{\partial fv}{\partial y}=0\,, \tag{3}$$

where u and v are the fluid velocity components in the x and y directions, respectively, ρ_l and ρ_s are the constant densities of liquid and solid, ρ is the variable density of the liquid, μ is the dynamic viscosity, p the pressure, g and Π split into x- and y-components of the acceleration due to gravity and the permeability of the solid, respectively, and f is the volume fraction of the liquid phase.

We find from experience that the solution of the mass and momentum equation (see below) on a staggered grid is stable if we solve for fu and fv. We therefore transform the advection term on the left hand side of (1) and (2). The derivative of the phase fraction that emerges is dropped as it appears only in the porous medium and fluid flow in the porous medium is dominated by the Darcy friction term. The resulting momentum equations are

$$\rho_l\left[\frac{\partial fu}{\partial t}+u\frac{\partial fu}{\partial x}+v\frac{\partial fu}{\partial y}\right]=\mu\left[\frac{\partial^2 fu}{\partial x^2}+\frac{\partial^2 fu}{\partial y^2}\right]-f\frac{\partial p}{\partial x}+f\rho g_x-f\frac{\mu}{\Pi_x}fu\,, \tag{4}$$

and

$$\rho_l\left[\frac{\partial fv}{\partial t}+u\frac{\partial fv}{\partial x}+v\frac{\partial fv}{\partial y}\right]=\mu\left[\frac{\partial^2 fv}{\partial x^2}+\frac{\partial^2 fv}{\partial y^2}\right]-f\frac{\partial p}{\partial y}+f\rho g_y-f\frac{\mu}{\Pi_y}fv\,. \tag{5}$$

From volume integration of the transport equation we obtain the conservation equations for heat and mass of solute. They are for heat

$$\bar{c}\frac{\partial T}{\partial t} + c_l u\frac{\partial T}{\partial x} + c_l v\frac{\partial T}{\partial y} = \overline{\left(\frac{k}{\rho}\right)}\left[\frac{\partial^2 T}{\partial x^2} + \frac{\partial^2 T}{\partial y^2}\right] - L\frac{\rho_s}{\rho_l}\frac{\partial f}{\partial t}, \tag{6}$$

and for solute

$$f\frac{\partial C}{\partial t} + fu\frac{\partial C}{\partial x} + fv\frac{\partial C}{\partial y} = f\Gamma\left[\frac{\partial^2 C}{\partial x^2} + \frac{\partial^2 C}{\partial y^2}\right] - C\frac{\partial f}{\partial t}. \tag{7}$$

In (6) and (7) T is the temperature of solid and liquid, C is the solute concentration in the liquid, L is the latent heat of fusion, and Γ is the solute diffusion coefficient in the liquid. Solute diffusion through the solid is neglected. The average quantities for the porous medium

$$\bar{c} = fc_l + (1-f)c_s \tag{8}$$

and

$$\overline{\left(\frac{k}{\rho}\right)} = f\frac{k_l}{\rho_l} + (1-f)\frac{k_s}{\rho_s} \tag{9}$$

are defined from the specific heat capacities c_l and c_s, and heat conductivities k_l and k_s of the liquid and solid, respectively. In the derivation of (6) we assume that the average temperatures of solid and liquid are equal and the same as the temperature at the microscopic solid-liquid interface. Further, latent heat is released or absorbed at the microscopic interface during phase transition. In the derivation of (7) we assume that the concentration of solute at the microscopic solid-liquid interface is equal to the average concentration of solute in the liquid, and that the concentration in the solid is zero. Solute is rejected into the liquid phase at the microscopic interface during the phase transition. We prescribe local thermodynamic equilibrium to determine the volume fraction f. The volume fraction is adjusted until the equilibrium condition,

$$T(f) = T_F(C(f)), \tag{10}$$

hold, where $T_F(C)$ is the freezing temperature as a function of solute concentration. We use a step-wise linear freezing point equation for sea ice, fitted to data given by Cox and Weeks (1982). Since on the scale of the finite volume simulation sea ice has a distinct transition form the purely liquid phase to the porous medium we incorporate a form of freezing front tracking. We restrict ice formation to those computational cells that either already contain ice or have a liquid volume fraction less than the specified threshold $f_f = 0.8$ [10] at a minimum of one of their faces. The liquid volume fraction at the cell face is estimated by linear extrapolation from neighbouring cells.

Equations (3) to (10) form a coupled set of differential equations that are solved iteratively for each time step with the SIMPLEC algorithm [16]. Discretisation of transient and advection term is limited to first order schemes in this work, as second

order schemes could not guarantee stability under all phase transition conditions studied. Since fluid velocities are quite small, first-order schemes give reasonably accurate results. We allow fluid inflow and outflow at the bottom of the domain. At this open boundary we chose the pressure boundary condition to enforce mass conservation, impose zero velocity gradient normal to the boundary, and zero velocity parallel to it [13]. Temperature and solute concentration at the open boundary take on prescribed values T_{OB} and C_{OB} for inward flow. The integrity of the algorithm is validated by correctly determining the critical Rayleigh number for Rayleigh-Bernard convection, and by calculating the flow pattern over a backward facing step in the laminar region of Reynolds number Re=800, where the open boundary is placed such as to intersect the second eddy [13].

PERMEABILITY FUNCTION

We seek a parameterisation of the permeability as a function of the liquid volume fraction f in order to solve the momentum equation. Since the governing equations are based on the assumption of an interconnected liquid phase, any isolated pockets have to be accounted for implicitly by the permeability function. Owing to the presence of drainage systems on all length scales, and the change of pore structure with age and history of the sea ice sheet [8] we cannot expect to find a permeability function of only one parameter that predicts the permeability in all circumstances. Here, we are particularly concerned with permeability in young sea ice under growth conditions, and find a permeability function for that situation.

Our primary concern in this paper is the modelling of sea ice desalination. Cox and Weeks (1975) have performed a laboratory study on the initial sea ice desalination process. They find that, after an initial brine segregation process, the salinity of the ice sheet continuously decreases mainly as a result of gravity drainage. They present data for f<0.7 that we fit with a power law function and obtain

$$\frac{\Delta S_{ice}}{\Delta t} = -4.2\times10^{-6}\ \text{psu m s}^{-1}\ \text{K}^{-1}\ \left(f-0.054\right)^{1.2}\ \frac{\Delta T}{\Delta z}, \qquad (11)$$

where the rate of sea ice desalination, $\Delta S_{ice}/\Delta t$, is proportional to the vertical temperature gradient, $\Delta T/\Delta z$. The rate of desalination is zero for $f \le 0.054$. Details of the fit are given in Petrich (2004). Assuming the change in salinity of sea ice is proportional to the solute concentration of sea ice, i.e. $\Delta S_{ice} = \beta\ \Delta C_{ice}$, and assuming that the temperature gradient is proportional to the concentration gradient of liquid brine, i.e. $\Delta T/\Delta z = \alpha\ \Delta C_b/\Delta z$, where α is the slope of the liquidus line, we rewrite (11)

$$\frac{\Delta C_{ice}}{\Delta t} = -4.2\times10^{-6}\ \text{psu m s}^{-1}\ \text{K}^{-1}\ \frac{\alpha}{\beta}\left(f-0.054\right)^{1.2}\ \frac{\Delta C_b}{\Delta z}. \qquad (12)$$

Comparing this expression to the transient and advection terms of the solute mass balance equation (7) we obtain an expression for the vertical liquid mass flux during freezing, *(f u)*, as a function of instantaneous liquid volume fraction f,

$$(fu) = -4.2\times10^{-6}\ \text{psu m s}^{-1}\ \text{K}^{-1}\ \frac{\alpha}{\beta}(f-0.054)^{1.2}. \tag{13}$$

We describe fluid flow during brine drainage by Darcy's law,

$$\Pi_c = \frac{\mu}{\nabla p}(fu) \tag{14}$$

with an isotropic permeability Π_c that is characteristic for the brine drainage process. Assuming that ∇p is approximately independent of the conditions of growth we obtain an isotropic permeability function for sea ice during initial desalination of the form

$$\Pi_c \propto (f-0.054)^{1.2}. \tag{15}$$

We fit the constant of proportionality in (15) so that the computer model yields realistic salinity profiles. In order to define what is realistic, reference salinity profiles are calculated from an expression for the stable distribution coefficient k_{eff} as a function of freezing front velocity v, where

$$\frac{S_{ice}}{S_0} = k_{eff} = 0.19\left(\frac{v}{1.35\times10^{-7}\ \text{ms}^{-1}}\right)^{0.46} \tag{16}$$

is a power law fit to the stable salinity data of Nakawo and Sinha (1981) from Arctic sea ice. The reference velocity of 1.35×10^{-7} ms^{-1} is the average freezing front velocity of that data. The justification for fitting a power law originates from the sea ice desalination model of Cox and Weeks (1988). Their model suggests [15] a power law relationship with exponent 0.42 for the range of ice growth velocities 3×10^{-8} ms^{-1} $< v <$ 3×10^{-6} ms^{-1}.

In an anisotropic medium the characteristic permeability Π_c in (15) can be understood as the path average of three orthogonal components, two horizontal components $\Pi_{x1,2}$ and one vertical component Π_y. In one instance Freitag (1999) finds a difference of almost one order of magnitude between the horizontal components Π_{x1} and Π_{x2} in columnar sea ice. However, we will continue to examine the suitability of an isotropic permeability to model sea ice growth.

EXAMPLE CALCULATIONS

We use the permeability function

$$\Pi_c = 1\times10^{-10}\ \text{m}^2\ (f-0.054)^{1.2} \tag{17}$$

for $f > 0.054$, and $\Pi_c = 1\times10^{-13}\ \text{m}^2$ for $f \le 0.054$.

Sea ice growth is simulated in domains of various aspect ratios, 320 to 1280 mm wide and 640 to 1920 mm high on square grids of cell size 20 x 20 mm^2, 40 x 40 mm^2, and 80 x 80 mm^2. Periodic boundaries [16] are imposed in the horizontal (x-direction), an open boundary at the bottom and the top is isothermal y-direction). The salinity of the water is 36 psu, and the water temperature is initially 1 mK above its equilibrium

freezing point. Water advected through the open boundary is at the same temperature and salinity as the water in the domain at the beginning of the simulation. Simulations are stopped when the freezing front reaches 240 mm above the open boundary. The details of the ice sheet growth simulation depend on the domain configuration. With horizontally periodic boundary conditions horizontal layers of fluid motion develop superimposed on the vertical brine drainage pattern, particularly in domains with few (e.g. 8) horizontal cells. Wider domains provide more opportunity for the brine to disturb this flow. These layers are artefacts of the two-dimensional domain. They are faster moving on fine grids than on coarse grids, probably because coarse grids increase localised mixing and dissipation of momentum. We find that high horizontal flow velocities reduce brine drainage in the systems investigated. To keep salinity profiles comparable, we limit horizontal flow velocities to 3 mms^{-1} by introducing an additional friction source term in the momentum equation. The choice of this limit originates in the observation that horizontal velocities of 3 mms^{-1} are seldom exceeded in simulations with 80 mm grid size. Feltham et al (2002) have developed an analytical model of ice growth in the presence of a shear flow and demonstrate that brine expulsion depends on shear stress in the fluid. Salinity profiles do not depend on the overall height of the domain. However, as expected, the smoothness of the horizontally averaged salinity profiles generally increases with increasing number of horizontal cells.

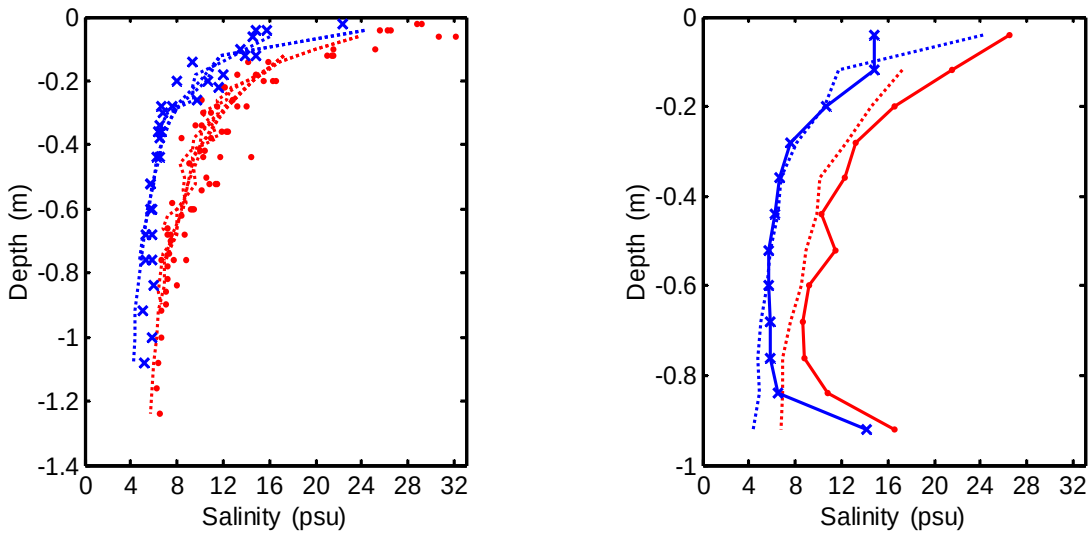

Fig. 1. Example of calculated salinity profiles for surface temperatures –10ºC (crosses) and –20ºC (dots). Dotted lines are profiles calculated from (16). (a) Superposition of 3 profiles at –10ºC and 5 profiles at –20ºC. The salinity close to the interface is not shown for clarity. (b) Single examples of ice sheet profiles including the ice-water interface obtained from a domain 1280 x 1280 mm^2, grid side 16 x 16. Note the different scales on the y-axes

Figure 1(a) illustrates the range of scatter obtained in calculations with various domain configurations mentioned above. Apart from the scatter the salinity profiles for ice grown from a constant temperature surface match the profiles predicted from (16) based on the interface velocity. The salinity closest to the ice-water interface is not shown for clarity. Figure 1(b) compares the salinity profile of an ice sheet grown at a surface

temperature of –10ºC with one grown in an otherwise identical domain configuration at –20ºC. Both profiles show the classical C-shape. While the profile of the simulated ice sheet at –10ºC coincides with the predicted profile from (16), the simulated profile at –20ºC is systematically higher than predicted by 1 to 2 psu. The latter profile shows deviations from a smooth curve at 0.35 and 0.5 m. An illustration of the nature of these deviations is given in Figure 2. It is apparent that the horizontal salinity distribution is very heterogeneous, and as such is qualitatively similar to naturally grown sea ice. Deviations in the calculated average salinity profile can usually be attributed to channel-like features, which have a salinity distinctly above the median of the ice sheet at that height.

SUMMARY

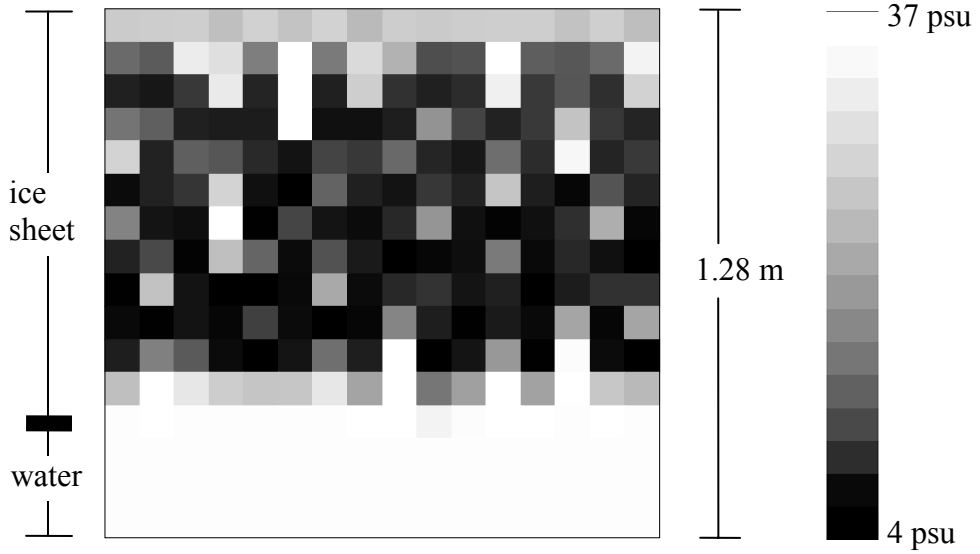

Fig. 2. Example calculation of ice growth at –20 °C surface temperature after 4 x 10^6 s. Grid size 16 x 16. The freezing front is in the range 0.96 to 1.04 m below the surface. The salinity of one of the white volumes 200 mm below the surface of the ice sheet is as high as 54 psu

We have demonstrated that it is possible to model sea ice growth and desalination as flow through a porous medium with phase change. The dynamics of the entire system is described by a single set of governing equations. We have estimated a permeability-porosity relationship from the observed correlation between rate of brine drainage, temperature gradient and liquid volume fraction *f*. Calculations with this permeability function resemble extrapolated data from the Arctic surprisingly well, although zero order approximations are made in the derivation, and the derivation does not account explicitly for an initial solute segregation [4]. The inhomogeneity of natural sea ice is resembled, including features such as brine channels. The form of the permeability function (17) corresponds to the power law expression predicted by percolation theory [9], where exponents of 1.2 to 1.3 are found for percolation in two-dimensional systems [1]. Unfortunately, the present model calculations are unable to distinguish whether or not it is mere chance that the exponent of equation (17) coincides with that for

percolation in a two-dimensional system. The success of the model in cases of simple, quasi one-dimensional sea ice growth allows its applicability to be tested in more complex situations.

ACKNOWLEDGEMENTS

This research was funded by Foundation for Research, Science and Technology, New Zealand. CP was financially supported by a University of Otago Post-graduate Scholarship. We thank Dr. Greg Leonard and Mr. Craig Purdie for a steady stream of feedback and suggestions during this project, and Prof. Hajo Eicken and Ms. Amy Heaton for insightful discussions.

REFERENCES

1. Berkowitz, B. and Balberg, I. Percolation approach to the problem of hydraulic conductivity in porous media. *Transport in Porous Media*, 9: 3, 275-286 (1992).

2. Cox, G. F. N. and Weeks, W. F. Brine drainage and initial salt entrapment in sodium chloride ice. *Cold Regions Research and Engineering Laboratory Research Report 345*, Hanover, NH, USA. (1975).

3. Cox, G. F. N. and Weeks, W. F. Equations for determining the gas and brine volumes in sea ice samples, *Cold Regions Research and Engineering Laboratory Report 82—30*, Hanover, NH, USA. (1982).

4. Cox, G. F. N. and Weeks, W. F. Numerical simulations of the profile properties of undeformed first-year sea ice during the growth season. *Journal of Geophysical Research 93*: C10, pp. 12449-12460 (1988).

5. Brinkman, H. C. A calculation of the viscous force exerted by a flowing fluid on a dense swarm of particles. *Applied Science Research A1*: pp. 27-34 (1947).

6. Eicken, H., Krouse, H. R., Kadko, D., and Perovich, D. K. Tracer studies of pathways and rates of meltwater transport through Arctic summer sea ice. *Journal of Geophysical Research 107*: C10, 8046, doi: 10.1029/2000JC000583 (2002).

7. Feltham, D. L., Worster M. G., and Wettlaufer, J. S. The influence of ocean flow on newly forming sea ice. *Journal of Geophysical Research 107*: C2, 10.1029/2000JC000559 (2002).

8. Freitag, J. The hydraulic properties of Arctic sea ice – Implications for the small scale particle transport (in German). *Berichte zur Polarforschung 325* (1999).

9. Golden, K. M., Ackley, S. F., and Lytle, V. I. The percolation phase transition in sea ice. *Science 282*: pp. 2238-2241 (1998).

10. Langhorne, P. J. and Robinson W. H. Alignment of crystals in sea ice due to fluid motion. *Cold Regions Science and Technology 12*: pp. 197-214 (1986).

11. Nakawo, M. and Sinha N. K. Growth rate and salinity profile of first-year sea ice in the high Arctic. *Journal of Glaciology 27*: 96, pp. 315-330 (1981).

12. Patankar, S. V. Numerical Heat Transfer and Fluid Flow, *Hemisphere Publishing Co.*, New York, NY, USA (1980).

13. Sani, R. L. and Gresho, P. M. Résumé and remarks on the open boundary condition minisymposium. *International Journal for Numerical Methods in Fluids 18*: pp. 983-1008 (1994).

14. Ono, N. and Kasai, T. Surface layer salinity of young sea ice. *Annals of Glaciology 6*: pp. 298-299 (1985).

15. Petrich, C. Refrozen cracks in sea ice. PhD thesis to be submitted, University of Otago, Dunedin, New Zealand (2004).

16. Versteeg, H. K. and Malalasekera, W. An introduction to Computational Fluid Dynamics: The Finite Volume Method. *Pearson Education Ltd.*, London, UK (1995).

17.Worster, M. G. Instabilities of the liquid and mushy regions during solidification of alloys. *Journal of Fluid Mechanics 237*: pp. 649-669 (1992).